Original

Pleskachevsky, A.; Dobrynin, M.; Babanin, A.V.; Guenther, H.; Stanev, E.:
Turbulent Mixing due to Surface Waves Indicated by Remote Sensing of Suspended Particulate Matter and Its Implementation into Coupled Modeling of Waves, Turbulence, and Circulation.
In: Journal of Physical Oceanography. Vol. 41 (2011) 4, 708 - 724.
First published online by AMS: 01.04.2011

http://dx.doi.org/10.1175/2010JPO4328.1

Turbulent Mixing due to Surface Waves Indicated by Remote Sensing of Suspended Particulate Matter and Its Implementation into Coupled Modeling of Waves, Turbulence, and Circulation

ANDREY PLESKACHEVSKY

German Aerospace Centre (DLR), Remote Sensing Technology Institute, and GKSS Research Center, Geesthacht, and Institute for Chemistry and Biology of the Sea (ICBM), University of Oldenburg, Oldenburg, Germany

MIKHAIL DOBRYNIN

GKSS Research Center, Geesthacht, Germany, and Centre for Ocean and Ice, Danish Meteorological Institute, Copenhagen, Denmark

ALEXANDER V. BABANIN

Swinburne University of Technology, Melbourne, Australia

HEINZ GÜNTHER

GKSS Research Center, Geesthacht, Germany

EMIL STANEV

GKSS Research Center, Geesthacht, and Institute for Chemistry and Biology of the Sea (ICBM), University of Oldenburg, Oldenburg, Germany

(Manuscript received 31 July 2009, in final form 9 September 2010)

ABSTRACT

This paper studies the impact of the surface waves on the turbulent mixing. The satellite observations of suspended particulate matter (SPM) at the ocean surface as an indicator of turbulent quantities of the flow are used. In a water column, SPM builds a vertical profile depending on settling velocities of the particles and on vertical mixing processes; thus, SPM is a perfect marker to study the turbulent quantities of the flow. Satellite observations in the North Sea show that surface SPM concentrations, in locations of its deposition, grow rapidly and build plume-shaped, long (many kilometers) uninterrupted and consistent structures during a storm. Also, satellites reveal that SPM rapidly sinks to the seabed after the storm peak has passed and wave height decreases (i.e., in the absence of strong turbulence).

The nonbreaking wave-induced turbulence has been discussed, parameterized, and implemented into an equation of evolution of turbulent kinetic energy (TKE) in the frame of mean-flow concept, which can be used in existing circulation models. The ratio between dissipated and total wave energy is used to describe the influence of wave damping on the mean flow. The numerical tests reproduce experiments in a wave tank very well and are supported by observations of SPM in the North Sea. Their results show that the motion of an individual nonbreaking wave includes turbulent fluctuations if the critical Reynolds number for wave motion is exceeded, independent of the presence of currents due to wind or tides. These fluctuations can produce high diffusivity and strongly influence mixing in the upper water layer of the ocean.

1. Introduction

In our paper, we analyze the effect of the motion induced by a nonbreaking wave on the turbulent mixing. Implementation of this effect for practical applications

Corresponding author address: Andrey Pleskachevsky, German Aerospace Centre (DLR), Remote Sensing Technology Institute, Oberpfaffenhofen, 82234 Wessling, Germany.
E-mail: andrey.pleskachevsky@dlr.de

DOI: 10.1175/2010JPO4328.1

requires coupling the wave, the turbulence, and the circulation models, which is also conducted. Because the topic is still quite new, the paper starts from a substantial introduction. In the current section, general and theoretical background is reviewed, and the methodology is described in section 2. Section 3 is dedicated to a key element of this paper, explaining and justifying the implementation of the nonbreaking turbulent diffusion produced by waves in circulation models. This implementation is then conducted and verified in section 4, where two experiments are considered and modeled. The first example is a laboratory test with the observed mixing in a wave tank, where the wave motion is the only energy source (other effects such as those caused by wind-induced currents, Langmuir circulation, etc., are not present), and the second series of tests is based on satellite observations in the ocean. Conclusions are summarized and discussed in section 5.

a. Background

Numerical simulation of different processes in the ocean, such as transport of different ingredients, chemical and biological exchange, morphodynamics, suspended matter transport, etc., is based on knowledge of wave climate and circulation current dynamics. Developments in recent years allow for application of such modern-designed circulation and ocean-wave models to simulate long time series of basic hydrodynamic and oceanographic parameters with fine spatial and temporal resolution. Imprecision of the model physics and parameterizations, however, can produce visible structural instability (McWilliams 2007) and in particular an imbalance when modeling variables that are able to accumulate the model inaccuracy [e.g., suspended particulate matter (SPM)]. Assimilation of data from different sources can improve the model results (e.g., Dobrynin et al. 2008), but it only highlights the need for employment of updated and more complete physics.

The turbulent diffusion is one of such basic physical processes and it plays an obvious key role in the vertical mixing action, which not only can be observed in the ocean but also can be demonstrated by experiments in water tanks. There are two apparent sources of turbulence in this case: the currents shear in the water column and near the bottom and the surface waves. Although the role of currents and the bottom boundary layer is well appreciated and well elaborated in the turbulence-mixing modeling, the role of the waves is routinely limited to injecting some turbulence under the ocean skin by means of wave breaking. It should be noticed, however, that the wave orbital motion is usually at least an order of magnitude faster than the currents and therefore should be able to generate turbulence directly. This source of turbulence is presently missing in most schemes for the upper-ocean mixing.

Langmuir circulation can be an additional course of the upper-ocean mixing (Langmuir 1938). Craik and Leibovich (1976) introduce the Langmuir circulation, which is caused by instabilities of the wave system in the presence of drift currents. Once formed, the Langmuir circulation can persist in the absence of wind (Craik 1982; Plueddemann et al. 1996; Phillips 2002), but it cannot persist in the absence of waves and is thus a wave-related phenomenon (see, e.g., Smith 1992; Phillips 2001a, 2003, 2005). Once present and fully developed, Langmuir cells would provide a vertical velocity, which can further facilitate the vertical mixing by bringing the turbulent surface waters all the way to the bottom of the mixed layer (e.g., Babanin et al. 2009). Dynamics of the mixed layer in presence of Langmuir circulation have been a subject of intensive studies by means of field measurements, laboratory experiments, and numerical simulations (e.g., Melville et al. 1998; Smith 1998; Phillips 2002). We should also mention the phenomenon of Langmuir turbulence proposed by McWilliams et al. (1997) and Sullivan and McWilliams (2010). In the present paper, we analyzed in detail two test cases: laboratory experiments and sediment suspension in the North Sea; in both cases, the mixing was clearly associated with the waves. In the laboratory, there was no Langmuir circulation present; the mixing by nonbreaking wave motion has been separated from other effects, investigated, and later verified in the North Sea environment.

b. Surface-wave motion and turbulence in circulation models

The main reason behind disregarding the wave-induced nonbreaking turbulence is the tradition to treat the surface wave motion as irrotational and therefore not able to produce shear stresses and turbulence directly. The concept of irrotationality, however, is a consequence of the initial theoretical assumption that the waves are free, they have no viscosity and surface tension, and therefore they cannot cause shear stresses (e.g., Komen et al. 1994). Such assumptions are helpful when obtaining analytical solutions for the wave motion in linear or nonlinear wave theories. Albeit small and negligible from the point of view of many applications, water viscosity, however, is not zero, and the existence of the wave-induced turbulence has been suggested (Babanin 2006). Such turbulence, in fact, is not a novelty to the wave modeling community. For example, the wave K model (Schneggenburger et al. 2000) uses turbulent diffusion as a dissipation source, parameterized through the Stokes drift (Rosenthal 1989).

The numerical modeling of hydrodynamic processes is separated into two basic disciplines: circulation modeling to simulate the mean flow (the computed currents present average values for all individual grid elements; dx, dy, dz,

and dt are the integration increments in space and time, respectively) and spectral wave modeling, which allows us to obtain statistical integral wave parameters such as significant wave height H_s and mean wave period T. Using such idealized obtained variables, which are averaged on a coarse spatial and temporal scale and simulated without correct coupling in terms of the energy balance (transfer of wave-energy dissipation from the wave to the circulation models), leads to the loss of some physical processes, depending on the application. For such applications as ocean-turbulence modeling, this means missing an additional source of turbulence, as well as additional turbulent diffusion in absence of breaking. However, most circulation models still do not take into account wave motion as a turbulence source.

According to linear wave theory, the idealized wave orbits are closed circles, and motion of water particles, temporally integrated, results in zero. As mentioned earlier, this lead to the general problem of modeling: different processes have different characteristic scales. The motion within an individual wave with properties H_s, T, and wavelength L occurs on spatial and temporal scales other than the scale used by circulation models; for example, the Hamburg Shelf Ocean Model (HAMSOM) circulation model implemented for the North Sea (Backhaus 1985; Pohlmann 1996) uses $dt = 5$ min (30 typical ocean-wave periods of $T = 10$ s) and spatial resolution 1.5′ (about 2.5 km: 17 wavelengths of $L = 150$ m). At the coarse mean-flow scale, these waves certainly return zero average currents. However, feedback to the coarser scale is required not only in terms of the integrated wave-related values but also in terms of the local finescale effects and dynamics. This can be done as a multiscale Reynolds decomposition. That is, the wave motion, which itself is a fluctuation at the scale of mean currents, at a smaller scale can be treated as mean motion subject to random turbulent fluctuations of its own.

c. *Turbulent diffusion and surface waves*

There is accumulating experimental evidence that wave-induced nonbreaking turbulence does exist. Yefimov and Khristoforov (1971) concluded that their measurements provide ‘‘a basis for assuming that small-scale turbulence is generated by the motion of waves of fundamental dimensions.’’ Estimated breaking rates of 0.4% and 0.01% for their records are negligible (Babanin 2006). Cavaleri and Zecchetto (1987) in their dedicated and thorough measurements of wave-induced Reynolds stresses gave explicit accounts for the wave breaking. One set of their data corresponds to active wind-forcing conditions (many breakers present are mentioned), whereas the other set describes steep swell (no breaking). Nonzero vertical momentum fluxes in absence of breaking were evident. Cavaleri and Zecchetto concluded that ‘‘in the water boundary layer, there can occur an additional mechanism of generation of turbulence... full, correct description of the phenomenon is still lacking.’’

Recently, in the ocean measurements, Gemmrich and Farmer (2004) reported presence of turbulence at a pre-breaking state of a wave, and Gemmrich (2010) demonstrated rates of turbulent energy dissipation in the definite absence of wave breaking, consistent with laboratory measurements by Babanin and Haus (2009). Babanin et al. (2005) conducted simultaneous measurements of the surface wind energy input rate and the wave-energy dissipation in water column of a finite-depth lake. They showed that, once the waves were present and even in absence of wave breaking, turbulence persisted through the entire water column and not only in the shear boundary layers near the surface and bottom. Babanin (2006) and Babanin and Haus (2009) described laboratory experiments with unforced (in the absence of wind), mechanically generated monochromatic deep-water waves. Thus, sources of the shear production were carefully eliminated, but turbulence was present and its intensity was measured to correlate with the wave height. Quantitatively, Babanin and Haus (2009) emphasized that the turbulence–dissipation rates they measured were instantaneous values incurred intermittently at the rear face of the waves; therefore, the average values have to be scaled down over the period of the wave and the period of the intermittency.

Indirect proof of the concept of wave-induced turbulence was further provided by recent laboratory experiments and numerical simulations of the upper-ocean mixing. Dai et al. (2010) conducted experiments in a wave tank with a stratified fluid and found that, in the presence of gentle waves on the water surface, the mixing was some two orders of magnitude faster than in the case of the mixing due to molecular diffusion. Qiao et al. (2004, 2010) introduced wave-induced stresses in ocean-circulation models coupled with surface waves and achieved dramatic improvements in predictions of the upper-ocean thermal structure and mixed layer depth compared to the traditional mixing schemes. Some theoretical works (e.g., Phillips 2001b; Ardhuin and Jenkins 2006) suggested mechanisms of wave–current–turbulence interactions that are capable of explaining transfer of energy from mean orbital motion to the turbulence, provided that background turbulence already exists.

d. *Suspended particulate matter in the North Sea as an indicator of turbulent diffusion*

In many satellite-borne ocean color images of the North Sea, a plume-like pattern is visible, which is caused by scattering the reflected sunlight at the SPM (for the definition, see appendix A) in the upper-ocean layer (Doerffer

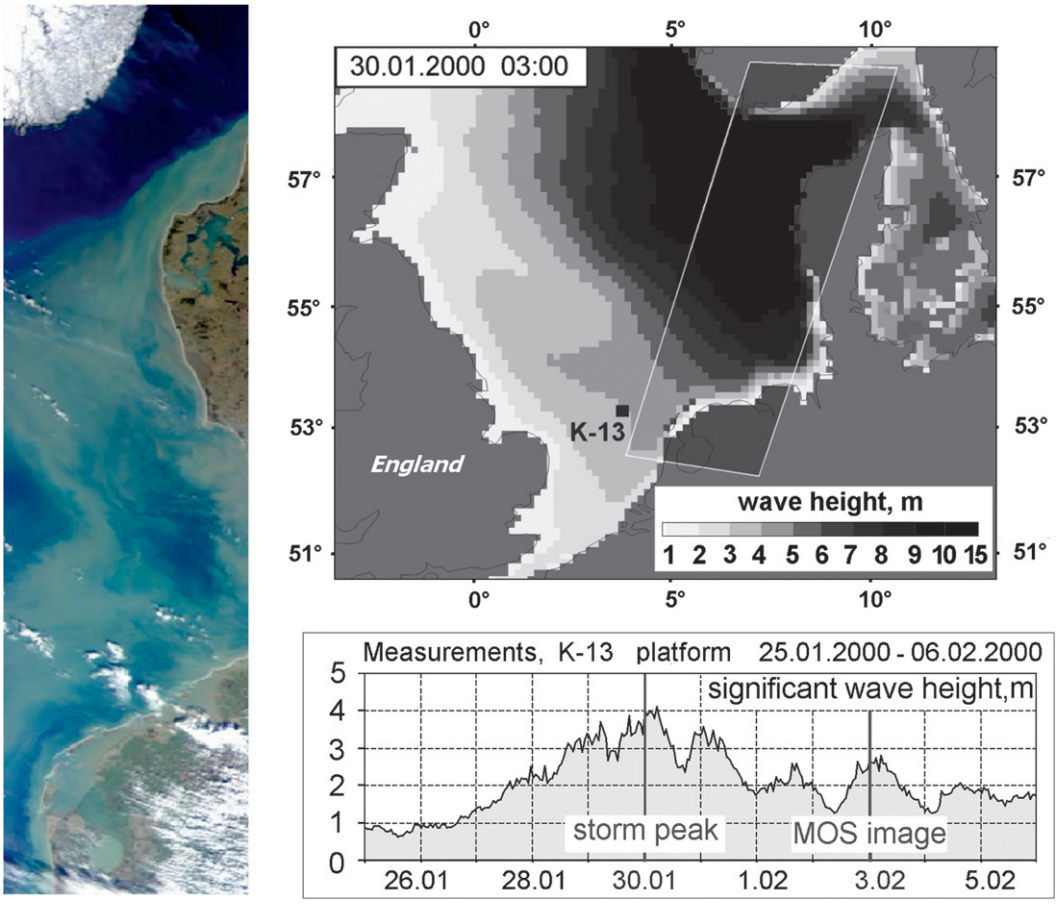

FIG. 1. Storm events in the North Sea at 29 Jan–4 Feb 2000 (the storm peak was at about 0300 UTC 30 Jan 2000). (left) Optical MOS image of German Bight on 3 Feb 2000 and (right) significant wave height in the North Sea at the storm peak.

and Fischer 1994). Such structure with SPM concentration about 10–50 mg l^{-1} (a typical concentration for calm weather conditions is 0–5 mg l^{-1}) can be seen with different intensity and it is clearly visible in the German Bight after storm events. Figure 1 (left) presents, for example, the surface SPM distribution during a storm in the German Bight delivered from satellite [Modular Optoelectronic Scanner (MOS)], and the corresponding wave conditions on the right: the wave fields are computed by the German Weather Service (DWD) using the Wave Model (WAM) (Günther et al. 1992) at a spatial resolution of 6 nautical miles.

The southern North Sea (Fig. 2a) is a shallow region with an average depth of about 40 m. This region has high fine-sediment content in the seabed, typically accumulated in the deeper areas like channels and trenches. These sediments can be resuspended and eroded because of storms, and a plume-shaped structure builds up at the surface at the location. Figure 2b presents the SPM concentration derived from MOS optical image (Fig. 1) after the storm on 1–3 February 2000. Close connection between surface structure of SPM and fine-sediment content in the seabed demonstrate the origin of this structure (surface SPM concentration field and isolines of bottom deposit).

The newest studies of remote sensing data confirm the findings based on single MOS images (e.g., Fig. 1; Pleskachevsky et al. 2002) that vertical mixing of the upper ocean significantly depends on waves. The entire 2003 dataset of satellite information from the Medium-Spectral Resolution Imaging Spectrometer [MERIS; on board the *Environmental Satellite* (*Envisat*); see appendixes B and C], which includes more than 400 MERIS scenes, was analyzed in our study. Commonly, available optical data do not present the storm peaks because of cloud coverage (wave height can reach more then 10 m, but the closest acquisitions is about 3 h after the storm peak). The circulation and waves are simulated for the North Sea (appendix D). The instantaneous measurements (all filtered 2003 data) in Fig. 3 show a connection between SPM and waves in area where the influence of circulation currents is not significant. In these areas, where

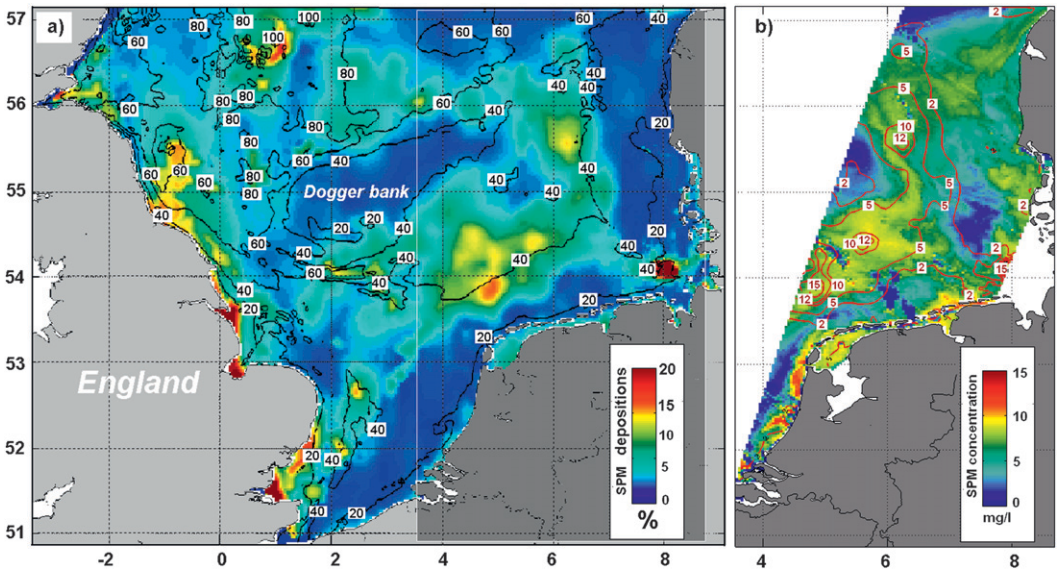

FIG. 2. (a) Seabed distribution of the fine-sediment (grain size, $O < 20$ μm) fraction (colors in percentage of sediment mass content) and bathymetry (lines; depth in meters) in the southern North Sea and (b) the surface SPM concentration derived from MOS with the typical plume-shaped structure (the optical image seen in Fig. 1) during the storm on 4 Feb 2000 (isolines show percentage of sediment mass content).

the fine-sediment content in the seabed is >8%, the surface SPM concentration rises immediately (Fig. 3b, area B) when significant wave height increases. A decrease in H_s leads to an immediate decrease in SPM concentration at the surface because of gravitational sinking. On the contrary, for the lower fine-sediment content in the seabed, an increase in the wave height (Fig. 3b, area A) does not lead to a visible increase in the surface SPM concentrations (for averaged storm conditions, change of the bottom fine-sediment content at 1% means a change of the surface SPM concentration at about 1 mg l^{-1} for the depth $d =$ 40 m because of erosion, which signifies mixing of the entire water column). This means maximal possible SPM concentration due to erosion at locations with high fine-sediment content, for average storm conditions. Summarized, the main feature of the wave influence is a strong and rapid mixing in the water column.

2. Methods and objectives

In this section, existing techniques aimed at accounting for wave–circulation interaction are summarized. Implementation of the new wave-induced turbulent mixing is discussed next. Then, objectives and method, to be followed in this study, are detailed.

a. Modeling the turbulence induced by wave–current interactions

Existing ocean-circulation schemes, which claim to have taken into account the waves but still assume that their orbital motion cannot cause the turbulence directly, can hardly reproduce such strong and prompt mixing as described in section 1d. One of such schemes refers to wave-breaking mechanism (Craig and Banner 1994). Wave breaking during a storm can indeed introduce strong turbulence, but this source of turbulence is limited to (injection into) the upper water layer and direct penetration of this turbulence is limited to the scale of the wave height (e.g., Gemmrich 2010). Its diffusion into the depth is too slow (if capable at all) to reach the depths of 30–50 m during a storm peak (e.g., Babanin et al. 2009). After the storm peak has passed, the waves are no longer high and steep enough to keep breaking, the whitecapping is too minor a turbulence source to influence the whole water column, and shear stress at seabed is no longer strong enough to hold SPM suspended at depths >30 m. As a result, within such a scheme, SPM starts sinking before its concentration at the surface can reach values actually observed.

Another known approach describes turbulence as an interaction of the Stokes drift with wind- and tide-produced currents (Ardhuin and Jenkins 2006), and it also is not capable of providing intensive and deep-reaching mixing. Furthermore, these approaches cannot in principle reproduce the simple experiment in a water tank (sections 3a and 4a; ink mixing due to nonbreaking waves, no wind, and no mean currents), which is our reference point. Indeed, the first approach requires wave breaking, which is not there, and the second one relies on the preexistence of the turbulence (e.g., due to wind forcing or currents that are also absent).

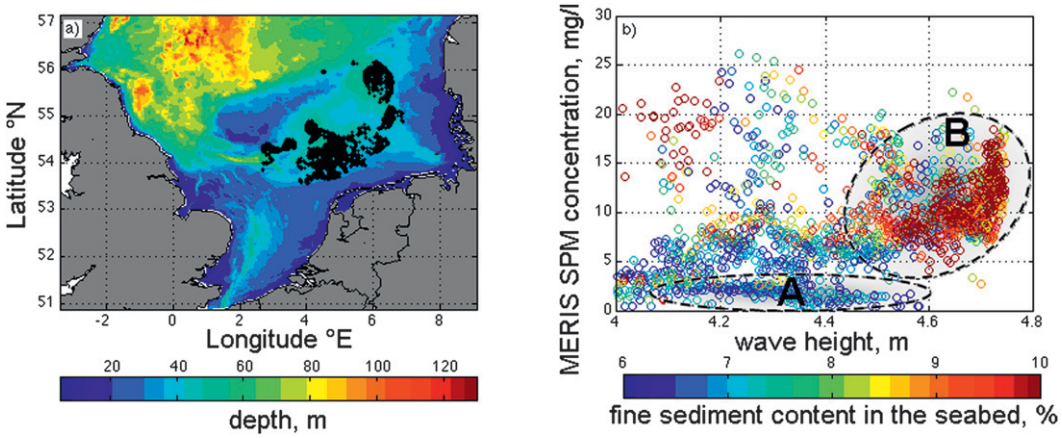

FIG. 3. (a) Selected areas (50 m > depth > 30 m; SPM content in the seabed >6%; and $H_s > 4$ m, black areas) on the topography map in the North Sea and (b) scatterplot of significant wave height and MERIS SPM concentration in these areas in 2003 [colors represent percentage of SPM mass content (grain size <20 μm) in the seabed].

Coupling of wave and circulation models through radiation stress is another way to account for influence of waves on turbulence. In this case, the spatial gradient of the wave energy is transferred to acceleration of mean currents. As a result, the current structure at the coast and around the sandbanks, where gradients of the wave energy are strongest, will undergo a significant change; for example, in the German Bight an along-shore current of some 30–50 cm s^{-1} magnitude appears in near-shore zone approximately 0.5 km wide. Local variations exceed 2 m s^{-1} if waves are completely dissipated because of large localized topographic gradients under storm conditions (Pleskachevsky et al. 2009). Turbulent properties of the water flow in such conditions are principally altered. However, attempts to fill the gap in energy balance in the system by means of such kind of coupling only (e.g., Warner et al. 2008) cannot reproduce wave-induced turbulence fully. By definition, the gradient of radiation stress reflects the spatial change of the total wave energy but not the local dissipations as such; that is, it does not take into account components in the net dissipation source term included in the wave model. This gradient is significant only in coastal areas or over sand banks. In the open sea, this gradient is nearly zero (dissipated energy is compensated by, e.g., wind input), and the structure presented in Fig. 1 cannot be reproduced through the radiation-stress coupling. Therefore, in order to simulate the influence of the wave motion on a flow field, wave-energy dissipation itself should be taken into account by circulation models.

b. *Wave-induced mixing and SPM modeling for the North Sea*

Modeling studies of SPM in the North Sea, using the SPM transport (SPMT) model developed at the GKSS Research Centre, have unambiguously shown that these plume structures (e.g., Fig. 1) are closely coupled with the vertical diffusion in the water column (Pleskachevsky et al. 2001). Turbulence due to the circulation currents was not strong enough to distribute the eroded SPM up to the surface, through about 40 m of the water column, during a short time window of the storm peak (6–10 h). A corresponding wave-based mixing coefficient was introduced and fitted empirically to reproduce the observed structure in the model. In the course of tuning, it emerged that the wave coefficient should be proportional to the wave amplitude (i.e., wave orbital velocity) squared and therefore to the wave energy (Pleskachevsky et al. 2001, 2005). Thus, the wave influence was taken into account, in addition to the diffusivity produced by currents. These findings confirmed results of independent measurements (Pearson et al. 2002). In Qiao et al. (2004), an identical approach solves a problem of the mixed layer depth (MLD) in the global ocean. The SPMT model simulates one-dimensional (1D) SPM dynamics in the vertical water column box and was implemented into the circulation model by the German Federal Maritime and Hydrographic Agency (BSH) (Dick et al. 2001). Precalculated current data produced by the circulation model, and wave data produced by WAM (Günther et al. 1992) were used. The model is running by BSH and reproduces the measured concentration at surface well, particularly during storm weather conditions (Gayer et al. 2006). However, this coupling was a simple parameterization, integrated in one-way mode, and it was not connected with turbulence models.

c. *Objectives and approach*

As was outlined in introduction, the main purpose of this paper is to implement a simple method of connecting existing circulation and wave models. This would allow us to account for the wave-induced mixing 1) by using

standard wave-modeling outputs (e.g., significant wave height and mean currents) and 2) through a standard turbulence model.

First, we will test our method by trying to reproduce the basic process in a hydrodynamic system: turbulent mixing by nonbreaking waves demonstrated experimentally in a wave tank (Babanin 2006). In this experiment, ink (a passive tracer) injected into the tank was dissolved because of wave-induced orbital motion after a critical value of the wave Reynolds number was exceeded (no wind, no currents, no circulation or upwelling; see section 4a for more details). In this case, the wave orbital motion is the only source of energy for such turbulent mixing.

The second step is to implement the method for more complicated environment: mixing of SPM, which includes not only dissolving passive tracers as above but also settling the matter and eroding the slick. A typical behavior of SPM is the vertical profiling caused by gravitational sinking. Typically, the SPM concentration is smaller in the upper water layers than in the lower layers (e.g., Wyrwa 2003). This distribution depends on settling velocities and the vertical mixing processes and thus on the turbulence. Therefore, the SPM is a good indicator of turbulent mixing: it immediately makes visible not only a starting point of the mixing (SPM is redistributed vertically up to the surface) but also the drop of the latter (rapid sinking the particles in absence of strong turbulence). For validation and comparison, the remote sensing data were used, which allowed us to cover large areas concurrently and show spatial structures and distribution of SPM at the sea surface.

3. Implementation of turbulent diffusion by nonbreaking waves into a circulation model

In this section, we will formulate the influence of nonbreaking waves on the upper-ocean mixing. The goal is to implement the wave action directly in the equation of evolution of the turbulent kinetic energy (TKE), aiming to improve the circulation model by taking into account the wave-induced diffusivity.

a. Assumptions

Our reference point is that the real nonbreaking wave-induced motion differs from the idealized mean-motion orbits obtained from linear or nonlinear wave theories. Existence of random fluctuations with respect to such mean motion has been confirmed experimentally (Babanin 2006; Babanin and Haus 2009; Dai et al. 2010). These turbulent fluctuations produce a small dissipation of the wave energy, spent on the turbulence generation, but most importantly they facilitate turbulent mixing near the interface where such source of turbulence is significant enough. Because the wave energy (and orbital velocities) reaches very high values during a storm, a slightest loss of it, though relatively small for the waves, has a strong effect on the mean-flow properties through the respective turbulent mixing. Here, we will obtain a parameterization based on the idealized analytical solution of the wave motion and implement it into a turbulence model.

Two views on the wave motion have been considered in this regard separately. Here, we will label them symmetrical and asymmetrical motion:

1) The symmetrical oscillation of the individual waves: such applications are not new and different approaches have been already carried out (e.g., Jacobs 1978; Qiao et al. 2004; Gayer et al. 2006).
2) The asymmetry of the wave-induced water-particle motion, as a residual effect, can be included into the mean flow, and this possibility also has been already considered as well [e.g., Ardhuin and Jenkins (2006) obtain it by using interaction of the Stokes drift and wind-induced currents]. We postulate that both effects are important and must be taken into account, and the overall effect on turbulent diffusivity can be obtained based on an idealized solution (linear wave theory) if the dissipation of the wave is known (e.g., from measurement or modeling).

b. Turbulent and idealized wave motion, turbulent fluctuations, and dissipation

In fluid flows, the turbulence is described by the fluctuating velocity u_i' (e.g., Roberts and Webster 2002) for $i = x, y, z$ directions. The instantaneous velocity u_i is generally (also due to wave motion) presented as

$$u_i = \overline{u}_i + u_i', \tag{1}$$

where $\overline{u}_i$ is the mean fluid velocity (for wave motion, the integration increment should be $dt \ll T$). By definition, the time-averaged fluctuations u_i' are zero, but it influences turbulent viscosity ν_t and turbulent diffusion. If the turbulence intensity (means the relation $u_i'/\overline{u}_i$) is less than 1% of the mean flow, this is normally classified as low turbulence; 1%–5% corresponds to medium turbulence intensity; and greater than 5% is a high-turbulence case. Because wave orbital velocities are on the order of 1.5–3 m s^{-1} for typical storm condition (can exceed 5 m s^{-1} on storm peak), even the low-turbulence condition will signify mean current fluctuations on the order of 1.5–5 cm s^{-1} and can produce the turbulent mixing in orders higher than the last because of molecular viscosity or weak circulation currents (for the depths 30–50 m, about 0–0.20 m s^{-1} in the lower water layers of the North Sea).

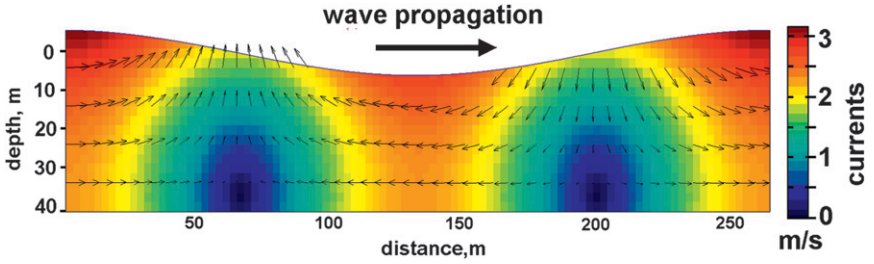

FIG. 4. Orbital wave motion. Velocity field produced by wave H_s = 10 m, T = 15 s, L = 265 m, and depth = 40 m based on the linear theory. The magnitude of velocity vector is shown by the color.

The average orbital velocity $\overline{u_{\mathrm{orb},\iota}}$ is a solution of linear theory, a function of H_s and T (see Fig. 4), and a particular case of $\overline{u}_i$ above. Input of H_s and T into $\overline{u_{\mathrm{orb},\iota}}$ (which is how the wave information is transferred into the circulation modeling) presents static values for the wave height, period, and length, whereas these properties change dynamically: such input does not include information about wave-energy dissipation of any kind. Therefore, turbulent fluctuations and damping effects due to them (loss of energy) are not presented in the idealized $\overline{u_{\mathrm{orb},\iota}}$, which is usually used for the technical applications.

In reality, even at laminar motion the idealized $\overline{u_{\mathrm{orb},\iota}}$ will be slowing down because of molecular water viscosity ν_w (it can be also described using Navier–Stokes equations with a combination of viscous and Reynolds stresses; Komen et al. 1994). The difference can be denoted as u_{Ti},

$$u_{\mathrm{Ti}} = \overline{u_{\mathrm{orb},\iota}} - \overline{u}_i, \tag{2}$$

and characterizes deviation of the real mean orbital wave motion in viscous fluid from ideal nonviscous fluid (mean viscosity of water is $\nu_w = 1.2\text{–}1.8 \times 10^{-6}$ m^2 s^{-1} depending on temperature). While the wave Reynolds number $\mathrm{Re}^{\mathrm{wave}}$ (Babanin 2006) is below critical value, the wave-induced motion remains laminar and the turbulent viscosity $\nu_t = 0$ ($u_i' = 0$). If the damped component u_{Ti} overcomes a certain limit, $\mathrm{Re}^{\mathrm{wave}}$ exceeds the critical value and the wave motion becomes turbulent as known from experiments (Babanin and Haus 2009). Then, turbulent stresses $\tau = u'w' = \nu_t(\partial u/\partial z)$ will significantly enhance the total eddy viscosity, which is now $\nu = \nu_t + \nu_w$.

Now, we can find the turbulent viscosity ν_t produced by the resultant mean wave velocity $\overline{u}_i$ in (2). The turbulent diffusion feeds back to the water motion and thus takes into account the wave damping. Figure 5 presents a scheme of such motion to demonstrate the dissipation-damping influence of the fluctuations on the mean motion (in reality, this scheme is more complicated because of the wave-energy input from wind and because of wave-energy advection). Such dissipation was measured in experiments in water tank, and for waves with frequency $f = 1.5$ Hz its rate can be expressed as (Babanin and Haus 2009)

$$k^{\varepsilon}_{\mathrm{wave}}(z)\big|_{f=1.5\mathrm{Hz}} = 300a(z)^3, \tag{3}$$

where $k^{\varepsilon}_{\mathrm{wave}}$ is depth-dependent kinetic-energy dissipation rate and a is wave amplitude. Vertical integration of Eq. (3) provides the wave-energy dissipation rate per unit of water surface.

c. *Implementation of the wave-induced turbulence into a circulation model and mean flow*

As noticed, the approximated wave motion can be represented by the linear-theory outcomes. Keeping in mind that existence of u_{Ti} is physically and mathematically responsible for appearance of turbulence in the first place (in nonviscous fluid $u_{\mathrm{Ti}} \equiv 0$), we will further assume that the value of u_{Ti} itself is negligible compared to $\overline{u_{\mathrm{orb},\iota}}$: that is, $\overline{u}_i \approx \overline{u_{\mathrm{orb},\iota}}$. This way, it is possible to obtain ν_t by using the shear frequency $M^2 = (d\overline{u}_x/dz)^2 + (d\overline{u}_z/dx)^2$, based on the idealized motion $\overline{u_{\mathrm{orb},\iota}}$, which

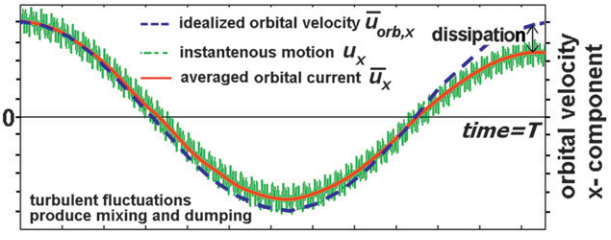

FIG. 5. Scheme of the wave damping by turbulent diffusion (no wind) for one orbital component during one wave period (horizontal axis is the time during T). The instantaneous motion u_x (green) includes fluctuations and results the averaged orbital current $\overline{u}_x$ (red), which differs from the idealized $\overline{u_{\mathrm{orb},x}}$ (blue) because of dissipation.

will subsequently be returned to the coarser mean-flow model. Using a linear wave theory (e.g., Svendsen and Jonsson 1982), the mean value (integrating over one wavelength) of shear frequency for the wave motion can be impressed as ($z = 0$ at the surface, positive direction is upward, and $k = 2\pi/L$ is the wavenumber)

$$\overline{M^2_{\text{wave}}}(z) = \left\{ \frac{k\pi H_s}{T} \frac{\sinh[k(z+d)]}{\sinh(kd)} \right\}^2. \tag{4}$$

Circulation models simulate the mean flow, and turbulence models interconnect mean currents U with its fluctuations U' through TKE K. The equation of evolution for K is (Burchard et al. 1999)

$$\frac{\partial K}{\partial T_{\text{mean}}} + U_i \frac{\partial K}{\partial X_i} = D_K + P_S + G - E_K, \tag{5}$$

where U_i is the mean-current component for i coordinate, G is the production of TKE by buoyancy, D_K is the turbulent and viscous transport term, and E_K is the dissipation term. The temporal and spatial resolution dT_{mean} and X_i correspondingly (capital letters) indicate the equation for the mean flow (i.e., simulate the process on scales that are coarser than the scale needed to simulate an individual wave with dt, dx_i). Here, P_S, in the default formulation of TKE Eq. (5), signifies TKE production by mean currents,

$$P_s = P_{\text{CURR}} = \upsilon_t M^2_{\text{CURR}}; \tag{6}$$

that is, M^2_{CURR} is the shear frequency due to the mean currents U_i. The eddy viscosity because of the mean-flow currents is usually defined as $\upsilon_t = \upsilon_{\text{CURR}} = c_\mu \sqrt{K} l$, with stability function c_μ and length scale l. The diffusivity D_t for turbulent mixing is defined through the turbulent Schmidt number $D_t = S_{\text{TSN}} \upsilon_t$.

Now, to take the wave motion into account, by the circulation model, we need to parameterize, and thus decompose the overall wave motion into two parts: subprocesses occur on a $dt < T$ micro time scale and mean-flow processes occur on a coarse dT_{mean} mean-flow scale. These subprocesses are referred to here as symmetric motion (SM), and the mean-flow processes are referred to here as asymmetric motion (AM):

1) If integrated, SM does not contribute to the mean currents (hence the motion is symmetric), but during dT_{mean}, on dt scale, a strong influence of waves on turbulence is possible. Impact of SM on the flow can be parameterized using shear $M^{\text{SM}}_{\text{wave}} = \overline{M}_{\text{wave}}$ from Eq. (4) (note that $\overline{M}_{\text{wave}}$ uses wave parameters H, T, and k: these integrated parameters will be obtained from the wave spectra after dissipation was taken into account in the wave model). Various implementations of this effect have been conducted before (e.g., Jacobs 1978; Qiao et al. 2004; Gayer et al. 2006).
2) AM represents the dissipation of the primary wave motion and results from temporal integrating: the orbital tracks are no longer closed because of this damping. The mean flow gains a weak residual-current effect. The asymmetric component can be parameterized by using shear $\overline{M}_{\text{wave}}$, as well as by employing the relation between wave-energy dissipation and total wave energy $k^{\text{AM}}_{\text{wave}}$,

$$M^{\text{AM}}_{\text{wave}} = k^{AM}_{wave} \overline{M}_{\text{wave}}. \tag{7}$$

Coefficient $k^{\text{AM}}_{\text{wave}}$ (which plays the role of the degree of efficiency) can be derived as the ratio of wave energy lost due to dissipation and total wave energy E_W,

$$k^{\text{AM}}_{\text{wave}} = \frac{E_{\text{diss}}}{E_w}, \tag{8}$$

where E_{diss} means the depth-integrated wave-energy dissipation (wave models consider vertical integrated water column and provide E_{diss} using dissipation sources; E_w is the total wave energy before dissipation is taken into account in wave model). This coefficient is nondimensional: that is, a fraction of wave energy passed to the wave-induced turbulence. The value $k^{\text{AM}}_{\text{wave}} \sim 1.5 \times 10^{-4}$ was obtained from measurements in the water tank experiment by integrating [Eq. (3)] vertically and using the exponential amplitude decay as a function of water depth. This mean value relates to wave steepness in the tank, which can then be related to the storm wave properties in the North Sea. Currently, to present the method we use this value for our calculations, but in the future it would need verifications in the field. The interactive coupling of the circulation, turbulence, and wave models by means of wave-energy dissipation will allow us to obtain this ratio with good accuracy [e.g., value of ratio in Eq. (8) varies between 1×10^{-3} and 1×10^{-7}, depending on wave steepness and depth for the turbulent diffusion dissipation term in the K wave model].

As noticed, the possibility to include the asymmetry of the wave-induced water-particle motion into mean flow has been considered before. The presented approach summarizes both effects (SM and AM).

First, we enlarge the TKE production by the wave source

$$P_{\text{wave}} = \upsilon_t (M^{\text{AM}}_{\text{wave}})^2 \tag{9}$$

(the asymmetric part of the wave motion that only connects to and influences the mean flow U directly),

$$P_s = P_{\mathrm{CURR}} + P_{\mathrm{wave}} = \upsilon_t[M^2_{\mathrm{CURR}} + (M^{\mathrm{AM}}_{\mathrm{wave}})^2]. \quad (10)$$

To account for the effect of the symmetric component, the resulting eddy viscosity must be modified by viscosity from the wave action υ_{wave} because of the subscale effects,

$$\upsilon_t = \upsilon_{\mathrm{CURR}} + \upsilon_{\mathrm{wave}}. \quad (11)$$

We apply the standard classical approach (e.g., Kapitza 2002; Casulli and Stelling 1998) and express υ_{wave} as follows:

$$\upsilon_{\mathrm{wave}} = l^2_{\mathrm{wave}} M^{\mathrm{SM}}_{\mathrm{wave}}, \quad (12)$$

where l_{wave} is the length scale for the wave-induced turbulence. The value of l_{wave} is assumed to be proportional to the wave amplitude, as a control characteristic of the wave motion,

$$l_{\mathrm{wave}} = a(z) = \frac{H}{2}\frac{\cosh[k(z+d)]}{\sinh(kd)}. \quad (13)$$

This assumption is confirmed by numerical modeling of Qiao et al. (2004), the experimental argument of Babanin (2006), and the model tests presented in the next section. Now, the TKE production P_s can be rewritten by taking into account the wave effects of both components,

$$P_s = (\upsilon_{\mathrm{CURR}} + \upsilon_{\mathrm{wave}})[M^2_{\mathrm{CURR}} + (M^{\mathrm{AM}}_{\mathrm{wave}})^2]. \quad (14)$$

This version of TKE production P_s describes the mean flow and includes the wave effects. The symmetric part of the wave motion (local effects) modifies the turbulent viscous term (influences the mean velocity U in terms of $dt > T$, through the eddy viscosity). The asymmetric part of the wave motion, due to dissipation of the wave energy, impacts the mean current directly and appears explicitly in the term for shear frequency.

To complete the approach, the Reynolds number and critical Reynolds number $\mathrm{Re}^{\mathrm{wave}}_{\mathrm{crit}} = 3000$ for wave motion were implemented from Babanin (2006),

$$\mathrm{Re}^{\mathrm{wave}}(z) = \frac{a(z)^2\omega}{\upsilon_w}, \quad (15)$$

where $\omega = 2\pi/T$ is wave angular frequency. To meet this condition, we set laminar motion for $\mathrm{Re}^{\mathrm{wave}} < \mathrm{Re}^{\mathrm{wave}}_{\mathrm{crit}}$ [the transition from laminar to turbulent motion can be indicated by maximal horizontal component of wave orbital velocity $u_{\mathrm{orb}}(z)$ on the order of 10–20 cm s^{-1}, depending on wave properties].

4. Results of numerical simulations

In this section, the experiments in the water tank were reproduced using the General Ocean Turbulence Model (GOTM) (Umlauf and Burchard 2003) first. Further down, we apply the method to simulations of the SPM mixing in the North Sea to compare the results with the satellite-derived data described in section 1.

a. Turbulent mixing of dissolved matter in a wave tank

1) EXPERIMENT

It has been confirmed experimentally that the wave-induced motion can be laminar and also turbulent, regardless of the presence of currents due to wind or tide. A simple experiment in a water tank (no wind and no currents) shows that wave-induced motions have turbulent fluctuations. As a result, the injected ink marker is diffused completely after the critical Reynolds number for wave motion (Babanin 2006) is exceeded [see Eq. (15)]. For this experiment, a single set of measurements was carried out for waves of 0.667-Hz frequency. The wave amplitude a changes gradually from 2 cm up to 4 cm and then down to 2 cm again. The water depth in the tank is approximately $d = 1$ m. Ink was injected into the water in the center of the tank:

> At $a = 0.02$ m, the motion is clearly laminar, with patterns of injected ink, while moving along the orbits, stayed unchanged for minutes. At $a = 0.03$ m, some vortexes became visible which eroded the upper parts of ink patterns. At $a = 0.04$ m, the motion was obviously turbulent, with the ink being completely dissolved within seconds after injection. When the amplitude was reduced down to $a = 0.02$ m again, laminar behavior of the traces was immediately restored as the source of turbulence was apparently removed. On the return way up to $a = 0.04$ m, onset of turbulence was observed at approximately the same wave amplitude as previously (Babanin 2006).

(See the photos in Fig. 6, left.) The observed effect is important for mixing in the ocean, too, and can be seen, in particular, through suspension of eroded sediment.

Numerical simulations presented below reproduce this experiment. For this test, the GOTM was used, with wave-induced mixing according to the above-presented method implemented.

2) SETUP

For the test, the wave amplitude a was being raised continuously from 0 to $a = 10$ cm during model time of 1 h ($T = 1.5$ s and depth $d = 1$ m). The turbulent Schmidt

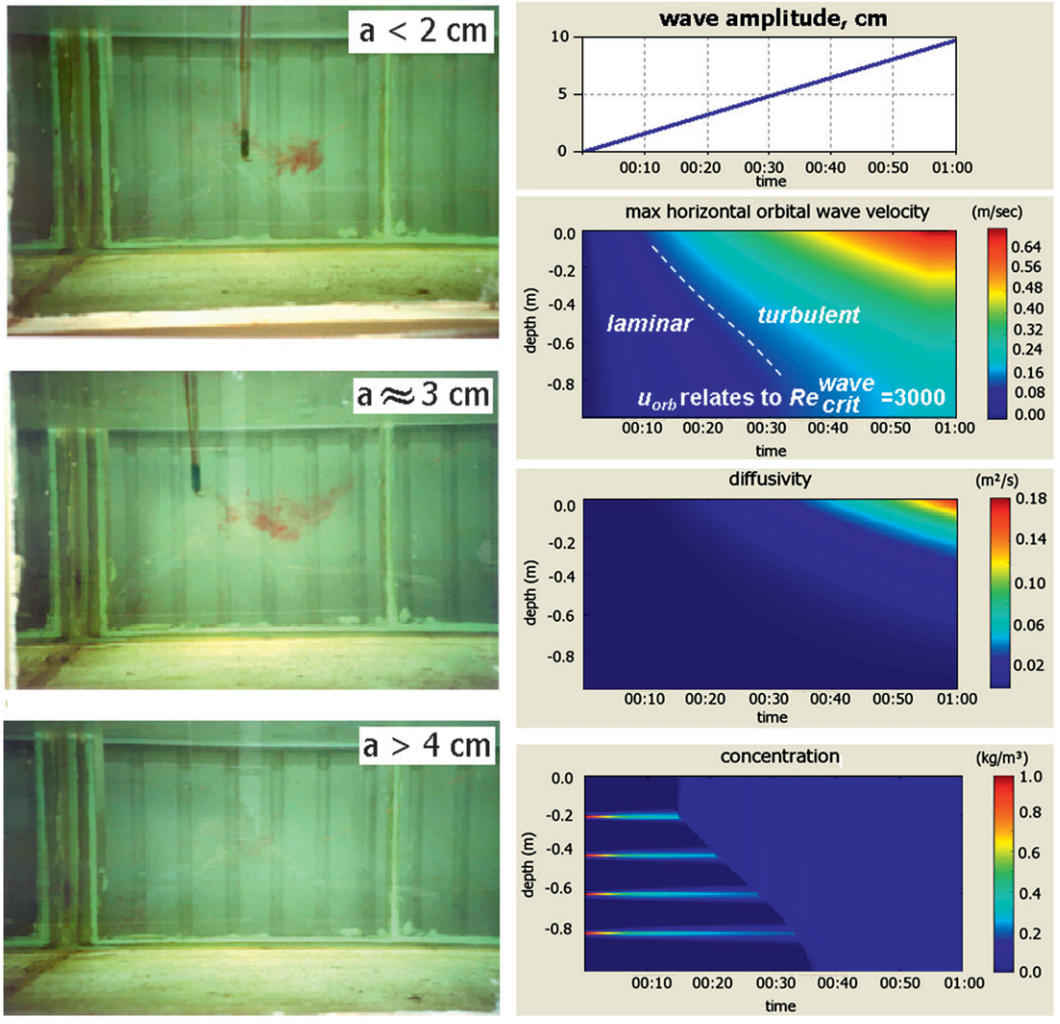

FIG. 6. Experiment in the water tank: (left) Ink is injected (no wind, no currents) for different wave amplitude and (right) reproducing of the experiment by numerical simulation.

number was set as $S_{TSN} = 1$ (nondimensional). Passive tracer is injected initially at depths of −0.2, −0.4, −0.6, and −0.8 m and an initial concentration of 1.0 kg m^{-3}.

3) RESULTS

Figure 6, right, presents the results of this numerical experiment. The four panels are (from top to bottom) wave amplitude a in centimeters (the control parameter), corresponding wave maximal horizontal velocity, wave-induced diffusivity, and concentration of the markers. In the beginning ($a < 2.5$ cm), only the tracer dissolution mediated by molecular diffusion is visible. Turbulent mixing, however, plays a key role when the orbital velocity exceeds the value of about 15 cm s^{-1} (thus exceeding $\mathrm{Re}_{\mathrm{crit}}^{\mathrm{wave}}$). With the wave amplitude reaching value of about 3 cm, the tracer initially starts to mix in the upper layers and later at $a \sim 5$ cm all the way down to the lowermost water layers ($dt = 0.1$ s and $dz = 1$ cm in the presented numerical experiment). Experiments with different dt (0.05–5 s) and dz (0.01–0.25 m) were carried out with identical results. Such outcomes reproduce the laboratory experiments of Babanin (2006) precisely.

b. *Wave-induced mixing during a storm event in the North Sea*

The SPMT model was incorporated into GOTM. Mixing and settling processes in the water column are simulated directly with GOTM. The implemented SPM block simulates the exchange processes between a water column and the sea bottom (sedimentation, resuspension, and erosion) and the processes in four layers of the uppermost 20 cm of the seabed (molecular diffusion and bioturbation). Erosion and sedimentation processes are driven by bed shear-stress velocity due to current and waves. For more

details, see appendix D and Gayer et al. (2006), Stanev et al. (2009), and Dobrynin et al. (2010).

Dynamics of the process is shown on Fig. 7. At the top right, two MERIS scenes present the SPM concentration at the surface on 3 April 2003 (1040 UTC, about 6 h after storm peak) and 3 days later.

1) FORCING DATA

For the numerical experiment, currents were simulated by the circulation model HAMSOM and waves by WAM (see appendix D). To study the erosion–turbulence processes, we use three locations (A, B, and C in Fig. 7a, top left; see also appendix C). The first line in Fig. 7b presents the control parameters [wave height H_s, mean wave period T_{m1}, wind speed W and surface currents (unnamed line)]; the SPM concentration derived from satellite (shown by red–yellow circles); and the modeled SPM concentration at the surface (red line) in A, B, and C.

2) INITIAL CONDITION

We assume that all SPM lies on the ground (see Fig. 2a). This assumption is coarse; but SPM, if available in the water column, should definitely be in the lowest water layer before the storm, which is not far from our approximation: the shear stresses at the seabed correspond to sinking and sedimentation for the depths $d >$ 30 m under calm weather condition in A, B, and C.

3) RESULTS

The last three lines in Fig. 7b provide details of the model results: the corresponding maximum of horizontal component of the wave orbital velocity, diffusivity and SPM concentration (three fractions of the SPM with different properties are simulated independently and then added up as the resulting concentration; see appendix D for details). The maximum of SPM erosion in the model corresponds to the storm peak. Eroded SPM are strongly mixed vertically, and the concentration at the surface rises rapidly during a very short interval (about 6 h) and reproduces, with a good quality, the process visible in the MERIS scene (Fig. 7a). Such an effect is practically not possible to be caused by currents for the water depth at the location (~43 m). Reaction time of the currents on the storm signal at the surface is too long, and the mean value of the currents and their shear at such a depth is not strong enough (about 0.1 m s^{-1}). The model test shows that the approach basically reproduces the processes correctly.

5. Conclusions

Water motion within an individual nonbreaking wave includes turbulent fluctuations, independent from presence of currents due to wind or tide, if the critical Reynolds number for wave motion is exceeded. These fluctuations can produce a high diffusivity and strongly influence mixing in the upper-ocean layer. If compared with the mean-flow processes simulated by circulation models, this motion occurs at the micro time and spatial scale. Therefore, although such motion can produce strong turbulent diffusivity, it cannot be seen by the standard mean-flow approach directly, using equations that describe the coarse-scales processes. Exact simulation of the diffusivity due to nonbreaking wave motion can be obtained by numerical hydrodynamic modeling, but it is necessary to take into account the fluid motion at all scales, including wave oscillations with temporal resolution $dt \ll T$ (wave period) and spatial resolution $dx \ll L$ (wavelength).

In the paper, we presented a parameterization method to include the nonbreaking wave effect on turbulence into a TKE equation, in the frame of the mean-flow concept. The method was then applied it in the turbulence model (to assimilate it into standard circulation models such as HAMSOM or the BSH circulation model). According to this method, the wave motion can be separated into two parts. The symmetric motion is due to orbital velocity, which reaches values of 5–7 m s^{-1} and, if integrated over time, results in zero mean current but strong local turbulence (Reynolds decomposition). The asymmetric motion relates to the ratio between dissipated and total wave energy and can be used to describe the influence of wave damping on mean flow. Currently, we obtain this ratio by using measurements or simulations of the wave dissipation. Interactive coupling of the circulation and wave models through the wave-energy dissipation will allow obtaining this dynamic ratio between wave dissipation and the total wave energy.

Implementation of satellite data from MERIS provides a new perspective because it yields the knowledge about SPM distribution during different weather conditions over extended sea surfaces. Data derived from MERIS (2003) confirm the earlier suggestions based on MOS single images that the vertical mixing of the upper ocean significantly depends on the waves. The MERIS images during and after storm reveal that the SPM concentration at the surface in the locations where sediment bottom deposits are presented grows immediately after the storm peak and reduces rapidly after the wave height drops down. The presented method of implementation of the wave impact on turbulent mixing reproduces these observed effects very well.

Acknowledgments. This study was supported by German Aerospace Centre DLR, GKSS Research Centre, Germany (BMBF project "Cli-Wa-Coas: Climate change, wind-wave interaction and anthropogenic impact on coastal

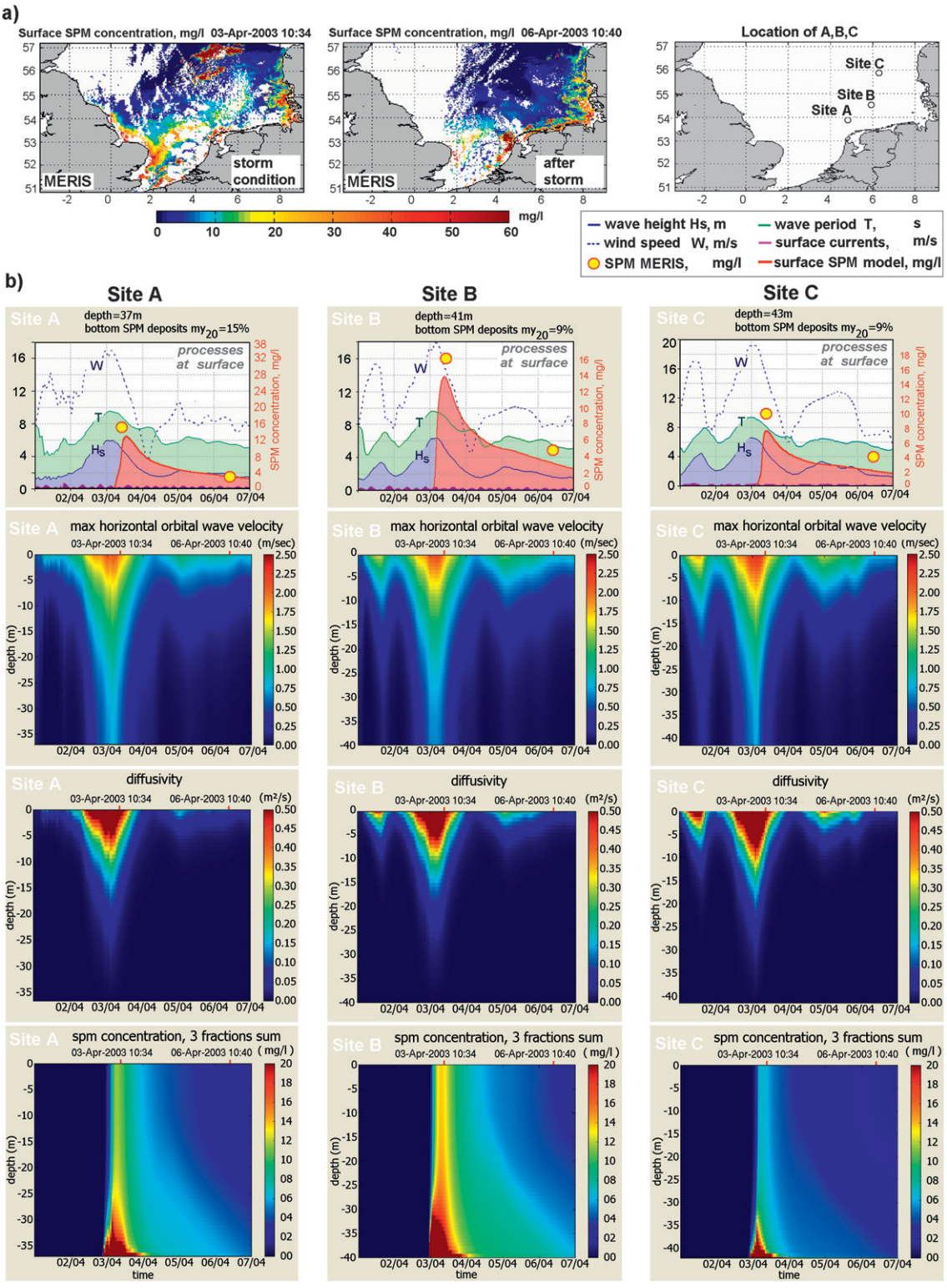

FIG. 7. The storm period 1–7 Apr 2003 in the southern North Sea. (a) MERIS scenes, presenting the SPM concentration at sea surface and locations of sites A, B, and C. The plume-shaped structure is visible during the storm but then disappears after the wave height sinks.

TABLE A1. Overview of sites A, B, and C used for the time series analysis (2003) and numerical simulations.

Location	A	B	C
Geographical position	53.90°N, 4.85°E	54.52°N, 5.90°E	55.9°N, 6.23°E
Depth (m; mean sea level)	37	41	43
Fine-sediment content in seabed (%)	15.4	8.7	8.5
Mean/max of wave height H_s (m)	1.4/8.7	1.4/9.4	1.6/10.4
Mean/max of surface currents (m s^{-1})	0.27/0.96	0.24/0.79	0.15/0.45

processes'') and Institute for Chemistry and Biology of the Sea (ICBM), University of Oldenburg, Germany (project ''Biogeochemistry of watts: Synergy of observational data and 3D models: Dynamics and suspended matter transport''). AVB gratefully acknowledges financial support of the Australian Research Council and Woodside Energy Ltd. through Grant LP0883888.

APPENDIX A

Suspended Particulate Matter

Suspended particulate matter (SPM) is defined as fine solid inorganic particles suspended in water (definition by data processing from satellite information). SPM in seawater mostly originates from the fine sediment (mud) in the bottom and fluvial inflow. It is classified by grain sizes (Wentworth 1922; Krumbein and Sloss 1963) referred to as fine-sediment fractions. The most abundant are silt (4–63 μm) and clay (<4 μm). There are also larger (and heavier) fractions (>63 μm), such as sand or gravel.

APPENDIX B

MERIS

MERIS operates in the solar reflective spectral range (15 spectral bands in the 390–1040 Nm). SPM surface concentrations obtained from level-1b MERIS data are used. The data cover the southern North Sea in the year 2003 with a resolution of 1040 m × 1160 m (ESA 2008) and are processed by the MERIS Case-2 Regional Processor (Doerffer et al. 2006). The data are interpolated to the wave model grid with a resolution of 1.5′ in the southward direction and 2.5′ in the eastward direction.

APPENDIX C

Time Series of SPM (MERIS), Waves, and Circulation Currents

See Table A1 and Fig. A1: The SPM surface concentration is about 2–5 mg l^{-1} during calm and it rises up to 15–25 mg l^{-1} during a storm periods. Note that the currents (Fig. A1, subplots) do not change visibly under storm conditions, but oscillations of wave height correlate significantly with the SPM concentration (some points reflecting high concentration during calm weather can be explained by data processing errors because data processing cannot definitely distinguish SPM around clouds edge).

APPENDIX D

Models Used

The circulation currents are simulated by the Hamburg Shelf Ocean Model (HAMSOM) and waves estimated with the ocean-wave spectrum Wave Model (WAM). The region of interest is the southern North Sea from 50.87° to 57.17°N and from 3.40°W to 9.10°E. Both models are integrated on the same grid with the horizontal resolution of 1.5′ in the north–south direction and 2.5′ in the east–west direction (corresponding to 2.5–3 km). Meteorological forcing for the models HAMSOM and WAM is based on hourly data provided by the Regional Model of Atmosphere (REMO; Feser et al. 2001). It includes the two wind components, atmospheric pressure, air temperature, relative humidity, and cloudiness. The model runs were performed for the year 2003.

HAMSOM model is a baroclinic, primitive equation 3D ocean-circulation z-coordinate model (Backhaus 1985; Pohlmann 1996).

WAM is a third-generation wave spectral model, which solves the wave transport equation explicitly without any a priori assumptions on the shape of the wave-energy spectrum (Günther et al. 1992; Komen et al. 1994). WAM is a state-of-the-art spectral wave model specifically designed for global and shelf sea applications.

The SPMT model simulates the processes of sedimentation, resuspension, and the exchange between water column and bottom. At the bottom, the model takes into account erosion, diffusion, and bioturbation. The forcing of erosion and sedimentation processes result from the

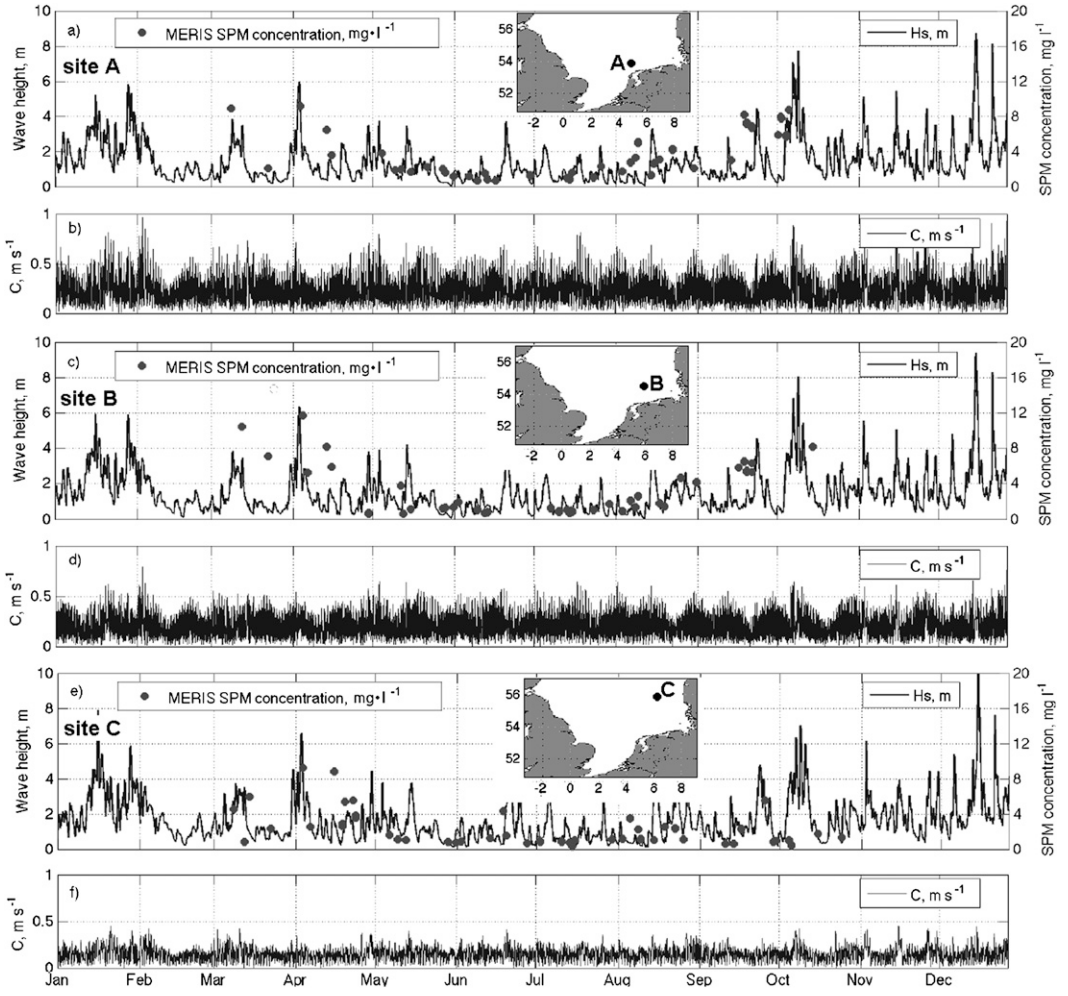

FIG. A1. Time series at A, B, and C in the North Sea in 2003 (geographical locations are shown on the map insets) of (a),(c),(e) MERIS SPM concentration (dots, right axis) and significant wave height (line, left axis). (b),(d),(f) Surface current velocity.

local shear-stress velocity derived in time and space under consideration of currents and waves according to Soulsby (1997). To reconstruct the reality for simulation of the seabed stress the significant wave height, H_s is temporally distributed according to Kokkinowrachos (1980), $H_N = H_s\text{SQRT}(\ln N/2)$ [e.g., $H_{500} = 1.76H_s$]. The model runs actually with three fractions of SPM (grain size < 63 μm) with different settling velocities. For calculations, the bottom sediment distribution data from Gayer et al. (2006) were used.

GOTM model (version 4.0) is a one-dimensional water column model for the most important hydrodynamic and thermodynamic processes related to vertical mixing in natural waters (for details, see documentation online at http://www.gotm.net). The standard test case ''wave-breaking scenario'' as background was used with ''switch off'' of the wind effects and ''switch on'' of the wave-induced turbulence: Eq. (14). Input of time series of the wave parameters was carried out correspondingly.

REFERENCES

Ardhuin, F., and A. D. Jenkins, 2006: On the interaction of surface waves and upper ocean turbulence. *J. Phys. Oceanogr.,* **36,** 551–557.

Babanin, A. V., 2006: On a wave-induced turbulence and a wave-mixed upper ocean layer. *Geophys. Res. Lett.,* **33,** L20605, doi:10.1029/2006GL027308.

——, and B. K. Haus, 2009: On the existence of water turbulence induced by nonbreaking surface waves. *J. Phys. Oceanogr.,* **39,** 2675–2679.

——, I. R. Young, and H. Mirfenderesk, 2005: Field and laboratory measurements of wave-bottom interaction. *Proc. 17th Australasian Coastal and Ocean Engineering Conf. and 10th Australasian Port and Harbour Conf.,* Adelaide, SA, Australia, NCCOE, IPENZ, and PIANC, 293–298.

——, A. Ganopolski, and W. R. C. Phillips, 2009: Wave-induced upper-ocean mixing in a climate modelling of intermediate complexity. *Ocean Modell.,* **29,** 189–197.

Backhaus, J. O., 1985: A three-dimensional model for the simulation of shelf sea dynamics. *Dtsch. Hydrogr. Z.,* **38,** 167–187.

Burchard, H., K. Bolding, and M. R. Villarreal, 1999: GOTM—A general ocean turbulence model. Theory, applications and test cases. European Commission Tech. Rep. EUR 18745 EN, 103 pp.

Casulli, V., and G. S. Stelling, 1998: Numerical simulation of 3D quasi-hydrostatic, free-surface flows. *J. Hydraul. Eng.,* **124,** 678–698.

Cavaleri, L., and S. Zecchetto, 1987: Reynolds stresses under wind waves. *J. Geophys. Res.,* **92,** 3894–3904.

Craig, P. D., and M. L. Banner, 1994: Modeling wave-enhanced turbulence in the ocean surface layer. *J. Phys. Oceanogr.,* **24,** 254–257.

Craik, A. D. D., 1982: The drift velocity of water waves. *J. Fluid Mech.,* **116,** 187–205.

——, and S. Leibovich, 1976: A rational model for Langmuir circulations. *J. Fluid Mech.,* **73,** 401–426.

Dai, D., F. Qiao, W. Sulisz, L. Han, and A. Babanin, 2010: An experiment on the nonbreaking surface-wave-induced vertical mixing. *J. Phys. Oceanogr.,* **40,** 2180–2188.

Dick, S., E. Kleine, S. H. Müller-Navarra, H. Klein, and H. Komo, 2001: The operational circulation model of BSH (BSHcmod)—Model description and validation. Bundesamt für Seeschiffahrt und Hydrographie Tech. Rep. 29, 49 pp.

Dobrynin, M., H. Günther, and G. Gayer, 2008: Assimilation of satellite data in a suspended particulate matter transport model. *Proc. US/EU-Baltic Int. Sym.,* Tallinn, Estonia, IEEE/OES, 4 pp, doi:10.1109/BALTIC.2008.4625513.

——, G. Gayer, A. L. Pleskachevsky, and H. Günther, 2010: Effect of waves and currents on the dynamics and seasonal variations of suspended particulate matter in the North Sea. *J. Mar. Syst.,* **82,** 1–20.

Doerffer, R., and J. Fischer, 1994: Concentrations of chlorophyll, suspended matter, and gelbstoff in case II waters derived from satellite coastal zone color scanner data with inverse modeling methods. *J. Geophys. Res,* **99,** 7457–7466.

——, H. Schiller, and M. Peters, cited 2006: MERIS Regional Case 2 water algorithms (C2R). [Available online at http://www.brockmann-consult.de/beam/software/plugins/merisc2r-1.1.zip.]

ESA, cited 2008: MERIS reduced resolution geolocated and calibration TOA radiance. European Space Agency. [Available online at http://envisat.esa.int/handbooks/meris/CNTR2-6.htm.]

Feser, F., R. Weisse, and H. von Storch, 2001: Multi-decadal atmospheric modeling for Europe yields multi-purpose data. *Eos, Trans. Amer. Geophys. Union,* **82,** 345–402.

Gayer, G., S. Dick, A. Pleskachevsky, and W. Rosenthal, 2006: Numerical modeling of suspended matter transport in the North Sea. *Ocean Dyn.,* **56,** 62–77.

Gemmrich, J., 2010: Strong turbulence in the wave crest region. *J. Phys. Oceanogr.,* **40,** 583–595.

——, and D. M. Farmer, 2004: Near-surface turbulence in the presence of breaking waves. *J. Phys. Oceanogr.,* **34,** 1067–1086.

Günther, H., S. Hasselmann, and P. A. E. M. Janssen, 1992: The WAM model cycle-4.0, User Manual. Deutsche Klimarechenzentrum Tech. Rep. 4, 102 pp.

Jacobs, C. A., 1978: Numerical simulations of the natural variability in water temperature during BOMEX using alternative forms of the vertical eddy exchange coefficients. *J. Phys. Oceanogr.,* **8,** 119–141.

Kapitza, H., 2002: TRIM documentation manual. GKSS Research Center Rep., 51 pp.

Kokkinowrachos, K., 1980: *Hydromechanik der Seebauwerke*. Vol. 15, *Handbuch der Werften,* Schroedter & Hauer, 167 pp.

Komen, G. I., L. Cavaleri, M. Donelan, K. Hasselmann, S. Hasselmann, and P. A. E. M. Janssen, 1994: *Dynamics and Modeling of Ocean Waves*. Cambridge University Press, 554 pp.

Krumbein, W. C., and L. L. Sloss, 1963: *Stratigraphy and Sedimentation*. 2nd ed. Freeman, 660 pp.

Langmuir, I., 1938: Surface motion of water induced by the wind. *Science,* **87,** 119–123.

McWilliams, J. C., 2007: Irreducible imprecision in atmospheric and oceanic simulations. *Proc. Natl. Acad. Sci. USA,* **104,** 8709–8713.

——, P. P. Sullivan, and C.-H. Moeng, 1997: Langmuir turbulence in the ocean. *J. Fluid Mech.,* **334,** 1–30.

Melville, W.-K., R. Shear, and F. Veron, 1998: Laboratory measurements of the generation and evolution of Langmuir circulations. *J. Fluid Mech.,* **364,** 31–58.

Pearson, J. M., I. Guymer, J. R. West, and L. E. Coates, 2002: Effect of wave height on cross-shore solute mixing. *J. Wtrwy. Port Coastal Ocean Eng.,* **128,** 10–20, doi:10.1061/(ASCE)0733-950X(2002)128:1(10).

Phillips, W. R. C., 2001a: On the generalized Stokes drift and pseudo momentum in a spectrum of rotational waves. *J. Fluid Mech.,* **430,** 209–220.

——, 2001b: On an instability to Langmuir circulation and the role of Prandtl and Richardson numbers. *J. Fluid Mech.,* **442,** 335–358.

——, 2002: Langmuir circulation beneath growing or decaying surface waves. *J. Fluid Mech.,* **469,** 317–342.

——, 2003: Langmuir circulation. *Wind over Waves II: Forecasting and Fundamentals of Applications.* S. G. Sajjadi and J. C. R. Hunt, Eds., Horwood, 157–167.

——, 2005: On the spacing of Langmuir circulation in strong shear. *J. Fluid Mech.,* **525,** 215–236.

Pleskachevsky, A., J. Horstmann, and W. Rosenthal, 2001: Modeling of sediment transport in synergy with ocean color data. *Proc. Fourth Berlin Workshop on Ocean Remote Sensing,* Berlin, Germany, Wissenschaft und Technick Verlag, 177–182.

——, G. Gayer, and W. Rosenthal, 2002: Numerical modeling of suspended matter transport. *Proc. 11th Int. Biennial Conf. on Physics of Estuaries and Coastal Seas,* Hamburg, Germany, GKSS Research Center, 476–479.

——, ——, J. Horstmann, and W. Rosenthal, 2005: Synergy of satellite remote sensing and numerical modeling for monitoring of suspended particulate matter. *Ocean Dyn.,* **55,** 2–9.

——, D. Eppel, and H. Kapitza, 2009: Interaction of waves, currents and tides, and wave-energy impact on the beach area of Sylt Island. *Ocean Dyn.,* **59,** 451–461, doi:10.1007/s10236-008-0174-1.

Plueddemann, A. J., J. A. Smith, D. M. Farmer, R. A. Weller, W. R. Crawford, R. Pinkel, S. Vagle, and A. Gnanadesikan, 1996: Structure and variability of Langmuir circulation during the Surface Waves Processes Program. *J. Geophys. Res.,* **101,** 3525–3543.

Pohlmann, T., 1996: Predicting the thermocline in a circulation model of the North Sea. Part I: Model description, calibration, and verification. *Cont. Shelf Res.,* **7,** 131–146.

Qiao, F., Y. Yuan, Y. Yang, Q. Zheng, C. Xia, and J. Ma, 2004: Wave-induced mixing in the upper ocean: Distribution and application to a global ocean circulation model. *Geophys. Res. Lett.,* **31,** L11303, doi:10.1029/2004GL019824.

——, ——, T. Ezer, C. Xia, Y. Yang, X. Lu, and Z. Song, 2010: A three-dimensional surface wave–ocean circulation coupled model and its initial testing. *Ocean Dyn.,* **60,** 1339–1355.

Roberts, P. J. W., and D. R. Webster, 2002: Turbulent diffusion. *Environmental Fluid Mechanics: Theories and Application,* H. H. Shen et al., Eds., ASCE Press, 7–45.

Rosenthal, W., 1989: Derivation of Phillips a-parameter from turbulent diffusion as a damping mechanism. *Radar Scattering from Modulated Wind Waves,* G. J. Komen and W. A. Oost, Eds., Kluwer Academic, 81–88.

Schneggenburger, C., H. Günther, and W. Rosenthal, 2000: Spectral wave modeling with non-linear dissipation: Validation and applications in a coastal tidal environment. *Coastal Eng.,* **41,** 201–235.

Smith, J. A., 1992: Observed growth of Langmuir circulation. *J. Geophys. Res.,* **97** (C4), 5651–5664.

——, 1998: Evolution of Langmuir circulation during a storm. *J. Geophys. Res.,* **103** (C6), 12 649–12 668.

Soulsby, R., 1997: *Dynamics of Marine Sands: A Manual for Practical Application*. Thomas Telford, 249 pp.

Stanev, E. V., M. Dobrynin, A. L. Pleskachevsky, S. Grayek, and H. Günther, 2009: Bed shear stress in the southern North Sea as an important driver for suspended sediment dynamics. *Ocean Dyn.,* **59,** 183–194.

Sullivan, P. P., and J. McWilliams, 2010: Dynamics of winds and currents coupled to surface waves. *Annu. Rev. Fluid Mech.,* **42,** 19–42.

Svendsen, A., and I. G. Jonsson, 1982: *Hydrodynamics of Coastal Regions*. Stougaard Jensen/Kobenhavn, 290 pp.

Umlauf, L., and H. Burchard, 2003: A generic length-scale equation for geophysical turbulence models. *J. Mar. Res.,* **61,** 235–265.

Warner, J. C., C. R. Sherwood, R. P. Signell, C. K. Harris, and H. G. Arango, 2008: Development of a three-dimensional, regional, coupled wave, current, and sediment-transport model. *Comput. Geosci.,* **34,** 1284–1306.

Wentworth, C. K., 1922: A scale of grade and class terms for clastic sediments. *J. Geol.,* **30,** 377–392.

Wyrwa, J., 2003: Modeling turbulence in stably stratified flows as part of cohesive sediment transport simulations in estuaries. Ph.D. dissertation, Technical University of Berlin, 220 pp.

Yefimov, V. V., and G. N. Khristoforov, 1971: Spectra and statistical relations between the velocity fluctuations in the upper layer of the sea and surface waves. *Izv. Atmos. Oceanic Phys.,* **7,** 1290–1310.